

Diffuse Ionized Gas in Edge-on Spiral Galaxies: Extraplanar and Outer Disk H α Emission¹

Charles G. Hoopes², René A. M. Walterbos²

New Mexico State University, Department of Astronomy, MSC 4500, Box 30001
 Las Cruces, New Mexico 88003
 choopes@nmsu.edu, rwalterb@nmsu.edu

Richard J. Rand

University of New Mexico, Department of Physics and Astronomy, 800 Yale Boulevard NE
 Albuquerque, New Mexico 87131-1156
 rjr@astro.phys.unm.edu

ABSTRACT

We present H α images of five edge-on galaxies: NGC 891, NGC 4631, NGC 4244, NGC 3003, and UGC 9242. We also analyze [SII] 6717+6731Å and [OIII] 5007Å images of NGC 4631. For several of these galaxies these images are the most sensitive to date. We analyze the ionized gas content, with particular attention to the diffuse ionized gas (DIG). The DIG layer in NGC 891 is traced out to at least 5 kpc from the midplane, confirming an earlier spectroscopic detection. The DIG in four of these galaxies contributes 40 to 50% of the total H α luminosity, similar to face-on galaxies, but in NGC 891 the DIG contributes 80 to 90%. This is likely due to the higher dust content in the disk of NGC 891 which obscures the HII regions, but may also reflect the extraordinary prominence of the DIG layer in that galaxy. Our very deep image of UGC 9242 shows very low surface brightness emission, as low as 0.3 pc cm⁻⁶, reaching 4 to 5 kpc above the midplane. This galaxy also exhibits filaments near the bright H α nucleus, an indication of a starburst superwind. In NGC 4631 we see a very large shell of emission extending 3.5 kpc into the halo. The [SII]/H α and [OIII]/H α ratios in NGC 4631 are consistent with the ratios seen in other galaxies, and with photoionization models. There is a region on the

¹Observations made with the Burrell Schmidt of the Warner and Swasey Observatory, Case Western Reserve University.

²Visiting Astronomer, Kitt Peak National Observatory, National Optical Astronomy Observatories, which is operated by the Association of Universities for Research in Astronomy, Inc. (AURA) under cooperative agreement with the National Science Foundation.

SE side of disk where the $[\text{OIII}]/(\text{H}\alpha + [\text{NII}])$ ratio reaches over 1.0 in the DIG, which coincides with an HI supershell. We use our very deep images of NGC 3003 and UGC 9242 to search for ionized gas in the outer disks as a test of the strength of the metagalactic ionizing radiation field. We find no outer disk emission down to our 1σ limit of 0.13 pc cm^{-6} on scales of 1.5 kpc in NGC 3003. Based on this limit we rule out a metagalactic ionizing radiation field stronger than $11 \times 10^{-23} \text{ ergs cm}^{-2} \text{s}^{-1} \text{Hz}^{-1} \text{sr}^{-1}$. There is an indication of extended disk emission in UGC 9242 which would imply a stronger radiation field, but various concerns, most importantly flatfielding uncertainties due to foreground stars in the image, lead us to question whether this feature is real.

Subject headings: Galaxies: Halos — Galaxies: ISM — Galaxies: Spiral

1. Introduction

Spiral galaxies contain a widespread layer of ionized Hydrogen, known as diffuse ionized gas (DIG, also called WIM for warm ionized medium). The properties of this component of the interstellar medium (ISM) are important for many aspects of galactic research, such as the influence of massive stars on the ISM, the porosity of the ISM, and the disk-halo connection. The Reynolds layer, as DIG in the Milky Way is known, has a filling factor of at least 0.2, and accounts for nearly all of the mass of ionized gas, equal to about 30% of the HI mass. DIG is less dense than HII regions ($n_e \sim 0.2 \text{ cm}^{-3}$, compared to 10^2 to 10^4 cm^{-3} in HII regions) but has a similar temperature ($\sim 8000\text{K}$). An excellent review of the properties of the Reynolds layer can be found in Reynolds (1990).

The $[\text{SII}] 6717+6731\text{\AA}$ to $\text{H}\alpha$ ratio is higher in the DIG relative to HII regions, while $[\text{OIII}] 5007\text{\AA}$ to $\text{H}\alpha$ is lower. In the Reynolds layer and in M31 the $[\text{NII}] 6548+6584\text{\AA}$ to $\text{H}\alpha$ ratio is about the same as in HII regions (Reynolds 1989; Greenawalt, Walterbos, & Braun 1997), while for NGC 891, the best studied edge-on galaxy, it appears to be higher in the DIG (Rand 1997a). These ratios can result from photoionization by a radiation field with a low ionization parameter U , the ratio of the photon density to the gas density (Mathis 1986; Domgörgen & Mathis 1994). However, transporting ionizing photons from HII regions to the DIG is still a problem, because of the long pathlengths that ionizing photons have to travel. In order to remain ionized, the Reynolds layer requires at least 15% of the Lyman continuum photons from OB stars in the Galaxy, equal to the amount of energy produced in supernovae. Studies of external galaxies suggest the requirement is even higher, consistently 30 to 50% (Walterbos & Braun 1994; Hoopes, Walterbos, &

Greenawalt 1996; Ferguson *et al.* 1996; Greenawalt *et al.* 1998). Whether this energy is leaking out of density-bounded HII regions, or can be provided by field OB stars is still an open question. Recent spectroscopic observations have challenged the photoionization models, including lower HeI 5876Å than predicted (Reynolds & Tufte 1995, Rand 1997b) indicating a softer ionizing spectrum than expected, higher [OIII] 5007Å in some galaxies than in others (Wang, Heckman, & Lehnert 1997; Martin 1997) and rising [OIII]/H α ratio with height in the halo of NGC 891 (Rand 1998). Shock ionization by supernovae is another source which likely plays a role at some level and may explain the anomalous [OIII] ratios, but it cannot provide enough energy to ionize the bulk of the DIG.

The Reynolds layer is vertically extended, with a scale height of 900 pc (Reynolds 1990). This distribution is quite different from that of OB stars, which have a scale height closer to 100 pc. H α imaging of external edge-on galaxies has revealed the presence of DIG with varying properties. The first galaxy to be studied was NGC 891, which has a very thick DIG layer that has been traced as far as $z=3.5$ kpc in imaging (Rand, Kulkarni, & Hester 1990, hereafter RKH; Dettmar 1990; Pildis, Bregman, & Schombert 1994), and $z=5$ kpc with spectroscopy (Rand 1997b). Several other galaxies possess smaller DIG layers, and others show very little extraplanar emission (Rand, Kulkarni, & Hester 1992; Rand 1996; Walterbos 1991). Filamentary structure is visible in the extraplanar emission of several galaxies, indicating an active disk-halo connection and illustrating a probable relation between DIG and star formation.

Here we present deep H α images of 5 edge-on galaxies. Some properties of these galaxies are given in Table 1. We attempt to address several questions with these images. First we would like to know the extent of the DIG layers in galaxies down to levels fainter than previously studied. The DIG in NGC 891 may extend even farther into the halo at very low surface brightness, and galaxies that do not show a bright DIG layer may in fact have faint extraplanar emission. This is important for understanding the structure of galaxies and their gaseous halos. Second, the correlation of DIG properties with other parameters of galaxies, such as star-formation rate or Hubble type, can be a clue toward the ionization source of the DIG, as well as the mechanism for cycling gas into the halo. The strengths of other emission lines can also provide information on the ionization source through comparison with models (*i.e.* Mathis 1986; Domgörgen & Mathis 1994). For this we obtained [SII] and [OIII] images NGC 4631.

Another goal of this project is to investigate the possibility of detecting H α emission from the outer disks of galaxies. Such emission is expected to occur when neutral Hydrogen in the outer disk and halo is ionized by the metagalactic radiation field (Silk & Sunyaev 1976). The observation of a sharp cutoff in the HI disks of several galaxies (NGC 3198

by Van Gorkom 1991; M33 by Corbelli, Schneider, & Salpeter 1989) provides indirect evidence that the outer disk gas may be ionized. Maloney (1993), Dove & Shull (1994) and Corbelli & Salpeter (1993) have modeled the situation, and they predict the emission to be very faint, from 0.2 pc cm^{-6} in emission measure down to 0.05 pc cm^{-6} (Maloney 1993). Fabry-Perot observations have pushed the observational limits close to the theoretical predictions (Bland-Hawthorn, Freeman, & Quinn 1997, Vogel *et al.* 1995). We obtained very deep images of two edge-ons, NGC 3003 and UGC 9242, for the purpose of searching for emission from the outer disk. Direct detection of ionized gas would allow the determination of the strength of the metagalactic radiation field at wavelengths below 912 Å, and would have important implications for cosmological models, for prospects of measuring rotation curves of galaxies at large radii, and for our knowledge of the structure of spiral galaxies.

The layout of this paper is as follows. In section 2 we detail the observations and data reduction techniques. In section 3 we describe the H α morphology of the galaxies in our sample. In section 4 we examine the DIG in these galaxies, including the vertical extent, and contribution to the total H α luminosity. In section 5 we discuss the [OIII] and [SII] images of NGC 4631. In section 6 we discuss the outer disk emission in NGC 3003 and UGC 9242. Section 7 contains a discussion of the implications of our results.

2. The Data

2.1. Observations and Data Reduction

The images discussed in this paper were obtained during several different observing runs at KPNO. A log of the observations is given in table 2. For all of the datasets we removed the bias level and bias structure using standard methods in IRAF. Twilight flatfields were combined into a super flatfield which was used to remove gain variations. In some cases (noted below) the galaxies were observed using the shift and stare technique, where the telescope is moved between exposures to place the galaxy on different regions of the chip. This allows the use of the image frames to produce a night sky flatfield, if the galaxy is small enough in the field of view of the telescope. We constructed a night sky flatfield by median combining the galaxy images after editing out the galaxy and foreground stars. The resulting image was heavily smoothed and then applied to the original images after flattening with twilight flatfields.

NGC 891 was observed with the Burrell-Schmidt telescope at KPNO in both H α and narrow-band continuum filters. Four pointings were observed and combined into a mosaic. The large field of view of the Schmidt ($1^\circ.15$) allowed us to make a night sky flatfield even

though NGC 891 is a relatively large galaxy ($12'$). The final flatfielding accuracy is about 1% across the images. NGC 891 was also observed with the 0.9 meter at KPNO, in $\text{H}\alpha$ and narrow-band continuum. Two pointings (out of 4 planned) were observed. NGC 891 is too big in the $23'$ field of view of the 0.9 meter to use the images to make a night sky flatfield, but five blank sky images were taken through the $\text{H}\alpha$ filter, with the telescope moved slightly after each exposure. These were combined to make a night sky flatfield which was then applied to the $\text{H}\alpha$ images. The continuum image was already flat to better than 1% without the use of a night sky flatfield.

We obtained $\text{H}\alpha$ and narrow-band continuum images of NGC 3003 and UGC 9242 using the 0.9m telescope at KPNO. All of the images used were taken during photometric conditions. The final mosaics consist of nine pointings for each galaxy. A few of the images of UGC 9242 had to be discarded due to large diffraction spikes from a bright star off of the image. The $23'$ field of view is large enough compared to these galaxies that the object images could be used to make a night sky flatfield, which provided a flatfielding accuracy for NGC 3003 of about 0.5%, and probably much better than this in the region the galaxy covers. The night-sky flat alone did not produce satisfactory results for the images of UGC 9242, but a second night sky flatfield made from observations of blank sky worked well on the remaining structure. The flatfielding uncertainty after this correction was about 0.5%, and as with NGC 3003 it is better over smaller scales.

NGC 4244 was observed at the KPNO 0.9 meter, during non-photometric conditions. Three 30 minute exposures in the same position were combined to produce the final image. NGC 4631 was also observed at the KPNO 0.9 meter in non-photometric conditions. A different detector was used, which provided a $6.6'$ field of view. Three pointings were required to cover the $14.3'$ length of NGC 4631, and these were combined into a mosaic during the reduction. The small field of view and necessity of mosaicing make it difficult to match background levels, hence flatfielding uncertainties may be larger than for the other targets. Each pointing consists of approximately 1.4 hours, with two pointings overlapping in the central field (roughly 7 arcminutes). Images of the central field were also obtained in [OIII] and [SII] filters.

The 0.9 meter observations of NGC 891, NGC 3003, and UGC 9242 were calibrated using observations of spectrophotometric standard stars. The Schmidt observation of NGC 891 and the 0.9 meter observations of NGC 4244 and NGC 4631 were calibrated using the R-magnitude of the galaxy. This was scaled by the response and transmission of the continuum filter and used to calibrate the continuum image. Then the stars in the line image were scaled to the continuum, taking into account the differences in the response of the filters. The [OIII] image of NGC 4631 was calibrated in a similar manner using the V

magnitude of the galaxy. For convenience, all of the $\text{H}\alpha$ images were converted to emission measure as if no [NII] was transmitted by the filter. The wide filter used on NGC 4631 contains the [NII] lines, but the narrow filters used for the other galaxies transmit very little [NII]. The [NII]/ $\text{H}\alpha$ ratio has been observed to vary from 0.6 to 1.1 in the DIG of NGC 891 (Rand 1997a). At the highest value, [NII] transmitted by the narrow filters contributes only 10–20% of the observed $\text{H}\alpha$ flux. For NGC 4631 we correct for [NII] where it is relevant.

2.2. Continuum Subtraction

One of the most uncertain procedures in analyzing emission line images is the removal of the underlying stellar continuum. Subtracting too little continuum will leave a faint background that can be interpreted as diffuse line emission, while subtracting too much continuum can remove a layer of real diffuse emission. These concerns can be minimized by observing the continuum close in wavelength to the line, but varying and unknown $\text{H}\alpha$ absorption produced by the stars in the galaxy makes a perfect subtraction difficult to achieve.

As a first determination of the continuum scale factor, we measured the fluxes of foreground stars in both images, and computed the factor needed to make them equal (for galaxies that were calibrated using the R magnitude, the fluxes are made equal during calibration). This relies on the foreground stars being of similar spectral type as the stars in the galaxy, which is not necessarily the case. We then visually inspected the images to be sure that there are no negative regions, and that there is no obvious component of the stellar continuum left in the image. For all of the galaxies the scale factor derived from foreground stars was satisfactory, except the [OIII] image of NGC 4631. For this image we adjusted the scale factor to achieve the best subtraction. To quantify the dependence of our analysis on the continuum subtraction, we vary the scale factor by $\pm 3\%$. At this level it is usually obvious that the continuum is incorrectly subtracted. Our results throughout this paper will include the variation in the continuum subtraction in the total uncertainty.

2.3. Scattered Light

Another potential problem with analyzing faint emission is the possibility of scattered light. Telescope optics produce halos around point sources, which could be mistaken for diffuse emission. In addition, dust within the galaxy itself may scatter light from HII regions, producing a halo of scattered light around HII regions. Walterbos & Braun (1994)

concluded that scattered light from within the galaxy is not a major component, based on the spectrum of the DIG. The [SII] to H α ratio is high in the DIG compared to HII regions, which would not be expected if the DIG were actually scattered light since the lines are very close in wavelength. Ferrara *et al.* (1996) modeled the scattering of HII region light by dust in the halo of NGC 891, and found it contributed only 10% of the DIG emission at 600 pc off the plane.

Methods of determining the contribution of scattered light from optics have been explored by Walterbos & Braun (1994) and Hoopes *et al.* (1996), and methods for correcting for scattered light have been used by RKH. Following these methods, we determined the possible contribution of scattered light from bright foreground stars in all of our images. We determined the radius in which 95% of the energy from the star is encircled, shown in table 2. Scattered light from HII regions will appear as halos around the regions to this radius, with only 5% of the light scattered further. We find that DIG extends further than this in all 5 galaxies, at a much higher level than 5%.

Scattered light can also affect the determination of the scale height of emission above the plane. To correct for this we deconvolved the images with the stellar point spread function (PSF). The PSF was measured using 10 stars in both the line and continuum images (except NGC 4631, where only 5 stars were suitable). The images were then deconvolved with the PSF using the Lucy-Richardson deconvolution algorithm with the task LUCY in IRAF. This was done before calibration and continuum subtraction. Vertical profile fitting was done on the deconvolved images (see section 4.1).

3. Results for Individual Galaxies

The H α images are shown in figures 1–5. The H α luminosities of the galaxies are listed in table 3. The correction for Galactic extinction (Burstein & Heiles 1984) is negligible for all of the galaxies except NGC891. The value listed in the table has been corrected; the luminosity before correcting for extinction is 2.8×10^{40} erg s $^{-1}$. No correction for internal extinction was made. The uncertainty given in the table is due to varying the continuum subtraction by $\pm 3\%$. Our H α luminosity for NGC 891 agrees well with Rand *et al.* (1992). Our flux for NGC 4631 is about 6% higher than that given in Rand *et al.* (1992), but our image contains [NII] emission as well, so our H α flux is actually lower. There are no published luminosities of NGC 3003, NGC 4244, and UGC 9242 with which to compare. NGC 4631 and NGC 4244 were observed during non-photometric conditions.

In this section we discuss the general appearance of the H α images. The H α morphology

of several of the galaxies in our sample have been discussed in great detail elsewhere, so we will keep our description brief. These include NGC 891 (RKH; Dettmar 1990; Pildis, Bregman, & Schombert 1994) and NGC 4631 (Rand *et al.* 1992; Golla, Dettmar, & Domgörden 1996). NGC 4244 was discussed briefly by Walterbos (1991) and Walterbos & Braun (1996). NGC 3003 and UGC 9242 have not previously been imaged in H α .

3.1. NGC 891

In figure 1 we show both the Schmidt and the 0.9 meter continuum subtracted H α images of NGC 891. Vertically extended emission is clearly present. The DIG layer can be traced to more than 3 kpc away from the plane in these figures. The emission seems fairly uniform, but does appear brighter and more extended near two large HII regions on the east side of the disk. In the higher resolution 0.9 meter image the extraplanar emission begins to show filamentary structure, although it is not as pronounced as in NGC 4631 (see below). There is a correlation with the brightest star forming regions, with the brightest DIG near bright HII regions in the inner disk. Rand (1997a) noted that the bright filaments almost always connect to an HII region in the disk.

3.2. NGC 3003

The morphology of this galaxy (figure 2) suggests that it may be disturbed, in that the spiral arms appear asymmetric. There is a small dwarf galaxy (or possibly a background galaxy) at the lower right edge of figure 2, but other than this there are no close companions visible in our images, which cover an area of 300×300 kpc at the distance of NGC 3003. However, just outside of our field of view is the small spiral NGC 3021. These two galaxies are separated by about 200 kpc in projected distance, and about 50 km s^{-1} in velocity (Tully 1988). The total H α luminosity of $1.18 \times 10^{41} \text{ erg s}^{-1}$ indicates that active star formation is ongoing. This H α luminosity is about an order of magnitude higher than for the starbursts NGC 253 and M82. In fact, of the galaxies observed by Young *et al.* (1996), one of the largest sample of galaxies observed in H α in the literature, only six of the 120 spirals have higher observed H α luminosities than NGC 3003 (not corrected for extinction). The H α image shows a bright nucleus, and many bright HII regions, including a very bright region in the outer western part of the disk. A projected spiral arm protrudes below the galaxy in the image, with a bright HII region at the end. The H α emitting disk is about 35 kpc across. The galaxy is not quite edge-on, so it is difficult to make any statements about the vertical extent of the DIG, though there is pervasive diffuse emission in the disk.

3.3. NGC 4244

This is a nearby galaxy (3.1 Mpc), so we can resolve a great deal of detail in the ionized disk. The HII regions distribution is extended in the vertical direction, a result perhaps of a weaker disk potential (Olling 1996). There are a few HII regions as far as 700 pc above the midplane. DIG is clearly visible in the disk, spread between several bright HII regions. It is immediately obvious, however, that an extensive DIG layer such as in NGC 891 is absent in this galaxy. Some short filaments exist in the central regions of the galaxy, but overall the DIG layer is confined to the disk. The galaxy appears quiescent in H α , and the low H α luminosity and low FIR surface brightness imply that there is relatively little star formation occurring. Most of the HII regions are small and faint, except for two bright complexes on either end of the disk. The absence of long bright filaments, such as those seen in NGC 891 and NGC 4631, imply that the galaxy also lacks any visible disk-halo interaction.

3.4. NGC 4631

The H α +[NII] image of this galaxy is shown in figure 4. An overlay of H α and x-ray emission for this galaxy, based on our data, can be found in Wang *et al.* (1995). There appear to be significant flatfielding uncertainties on the south side of the disk, near the bottom edge of the image, so we restrict our analysis to the north side. The image shows a disturbed disk, most likely due to an interaction with its companion galaxies NGC 4627 and NGC 4656. The disk appears to be actively forming stars, and the disk-halo interface is also very active in this galaxy. Rand *et al.* (1992) pointed out two bright vertical “worms” of emission east of the nucleus on the north side of the disk. We note that these worms are connected to longer, fainter filaments, and the western worm appears to curve back around toward the disk. There is an even larger loop of emission which surrounds the two worms (indicated by the arrows in figure 4). It begins just east of the easternmost worm and extends 3.5 kpc into the halo. Unfortunately there is a seam in the image where the loop might reconnect to the disk. The surface brightness at the top of the loop is about 12 pc cm $^{-6}$. The large loop is barely visible in the H α image presented by Rand *et al.* (1992, their figure 5). What appears to be another filament about 3 kpc east of the giant loop in our image is actually another seam. There is significant extraplanar emission in the form of discrete features such as the loops and worms, and a smoother component can be traced up to about 2 kpc on the north side. Donahue, Aldering, & Stocke (1995) detected a faint halo extending 16 kpc from the plane of NGC 4631, with a maximum brightness of 0.69 pc cm $^{-6}$ per square arcsecond. We could not confirm the detection because of the smaller field

of view of our observations. This emission is probably related to the high star formation and disturbed nature of this galaxy resulting from the tidal interaction, as it is too bright to be caused by the metagalactic ionizing radiation field.

3.5. UGC 9242

This galaxy appears to be close to exactly edge on (figure 5). The continuum image shows a very thin and symmetric disk. The H α emitting disk is about 35 kpc across. It has a bright nucleus in H α and several bright star forming regions. There are two plumes visible on the north side of the nucleus. They can be traced about 1.8 kpc from the midplane, with typical emission measures ranging from 20 just above the disk to about 5 at the highest point. These are probably associated with star formation in the nucleus, but it is not known whether these are two separate outflows, or whether they are the brightened edges of a conical outflow such as that seen in NGC 253 (Heckman, Armus, & Miley 1990). If it is a conical outflow, it is 1200 pc wide at the top. There is also some structure on the other side of the nucleus, which also may be 2 spurs of emission, shorter and weaker than the counterparts on the north side. This suggests a double sided outflow, with a morphology similar to the “H” shaped filaments seen in NGC 3079 (Hester *et al.* 1990; Veilleux, Cecil, & Bland-Hawthorn 1995) and NGC 4013 (Rand 1996). The bright nucleus is about 1 kpc across, with an H α luminosity in a 12''(about 1 kpc) diameter aperture of 4.2×10^{39} erg s $^{-1}$, comparable to the brightest HII regions in most galaxies (Kennicutt 1988), and in fact equal to the total H α luminosity of NGC 4244. Except for these filaments there is very little obvious extraplanar emission, and there is no evidence for disk-halo interaction beyond the nucleus, but like all of the galaxies in our sample the disk is filled with DIG.

4. The Diffuse Ionized Gas

4.1. Vertical Extent

Walterbos & Braun (1996) compared the appearance of the DIG layers in three of the galaxies in our sample, NGC 891, NGC 4244, and NGC 4631. Figure 6 is a more exact comparison, incorporating UGC 9242. The images are shown on the same spatial scale, brightness scale, and logarithmic stretch. The comparison shows the range of DIG morphologies. The most prominent example is the smooth, bright, extended layer in NGC 891. The patchy, filamentary layer in NGC 4631 may be related to recently enhanced star formation as a result of an encounter. The most common appearance of the DIG may be

more similar to the weaker layers in NGC 4244 and UGC 9242. The inclination of NGC 3003 hinders our analysis of the extraplanar emission.

Following RKH and Rand (1996), we have attempted to characterize the DIG as an exponential layer. We fit the vertical profile averaged over the central 10 kpc to increase the signal to noise. In order to avoid including light from HII regions in the fit, we excluded emission from $|z| \leq 300$ pc. NGC 4244 has a thicker disk of HII regions, so we excluded emission from $|z| \leq 500$ pc. We tried fits using a single exponential function as well as fits using two exponentials. The parameters of the best fits for three of the galaxies are given in table 4. The vertical profile of NGC 3003 suggests that it may also possess faint extraplanar emission, but the lower inclination of this galaxy make the detection uncertain, as such emission may arise from the outer part of the disk. We do not address it further here, nor do we attempt the analysis for NGC 4631 due to its disturbed nature and the poor flatfielding of the image. Note that the scale heights given are for the surface brightness (emission measure). The electron scale height is twice the emission measure scale height, assuming the emission is only H α . If much [NII] is included in the filter, a rising [NII]/H α ratio in the halo such as those observed in NGC 891 (Rand 1998) and NGC 4631 (Golla, Dettmar, & Domgörden 1996) could make the scale heights appear larger than they really are. The electron scale height for the Reynolds layer is 900 pc (Reynolds 1990).

Previous imaging of NGC 891 (RKH) has traced the extraplanar DIG to as far as 3.5 kpc from the plane of the galaxy. Spectroscopy (Rand 1997b) has traced the emission even further, to at least 5 kpc. Figure 7 shows a vertical profile of the deconvolved Schmidt H α image of NGC 891, averaged over the central 10 kpc. The emission can be traced as far as 5 kpc off the plane in both directions. Thus we confirm the spectroscopic detection. There is a suggestion that the emission continues even further, to as far as 7 kpc, on the west side of the disk. However, foreground stars in this part of the image make this uncertain. Although the two fits look quite similar in the linear scaling, the logarithmically scaled plot shows that two exponential functions better fit the faint component of the profile. For comparison, the stellar thin disk of NGC 891 has a scale height of 425 pc, and the stellar thick disk has a scale height of about 1.9 kpc from surface photometry (Morrison 1999; Morrison *et al.* 1997).

Even averaged over 10 kpc the extraplanar emission in NGC 4244 is very weak (figure 8). Using two exponential functions, we find one component with a very small scale height, about a factor of 2–3 lower than that of the Galaxy, and a fainter, broader component. The faint component may be due to a flatfielding problem, such as low level vignetting in the image. If we fit only one exponential the scale heights are closer to that of the Galaxy (450 pc). The two-exponential fit is statistically better, but both functions describe the emission

fairly well. NGC 4244 does not appear to possess a thick stellar disk (Morrison 1999).

Figure 9 shows that the extraplanar emission in UGC 9242 cannot be described by a single exponential layer. Using two exponential functions, the bright component of the vertical profile is well described by a relatively low scale-height exponential, as expected from the appearance of the $\text{H}\alpha$ image. However, there is a faint tail of emission which is clearly visible out to 3–4 kpc. The scale height of this component is similar to and perhaps even larger than the scale height of the Reynolds layer. As noted, UGC 9242 has bright filaments expending from the nucleus which may hamper the fit. In figure 10 we show the vertical profile of the central 20 kpc with the central 3 kpc excluded so as to remove the contribution of these filaments. The parameters of the model fits are shown in table 4. A single exponential still cannot fit the emission. The scale heights for the bright component are similar to the 10 kpc fit, but the faint components are even more extended. The high- z tail appears to extend well past 5 kpc.

In figure 11 we show the profiles of NGC 891, UGC 9242, and NGC 4244 overplotted with the best fit model for each. Although NGC 891 has a much brighter DIG layer than UGC 9242, extraplanar emission in both galaxies actually reaches comparable distances above the disk. NGC 4244 clearly has no extraplanar emission comparable to the other two galaxies. The logarithmically scaled plots clearly show that two exponential components make up the extraplanar DIG in NGC 891 and UGC 9242, and possibly also in NGC 4244.

Table 5 shows some parameters derived from the model fits. It is necessary to know the diameter of the DIG cylinder to derive these properties, so we estimate it from the $\text{H}\alpha$ images. The emission measure in a column perpendicular to the disk is given for each of the two components. We call the lower scale height component “thick disk” DIG (so as not to be confused with the HII region thin disk), and the higher scale height component “halo” DIG. The two components contribute nearly equally to the total perpendicular emission measure in NGC 891, while the halo components is weaker in the other two galaxies. The Galaxy resembles UGC 9242 in terms of total perpendicular emission measure and surface density, but keep in mind that the Galactic DIG parameters are derived for the solar neighborhood, while for the external galaxies these DIG parameters apply closer to the center where it is brighter. Following RKH, a constant filling factor of $\phi=0.25$ is assumed when calculating the surface density, although it may rise in the halo (Kulkarni & Heiles 1988). The surface densities include helium at solar abundance.

4.2. Diffuse Fractions

Another way to compare the DIG in different galaxies is through the diffuse fraction, which is the contribution of the DIG to the total $\text{H}\alpha$ luminosity. We use the same method used by Hoopes *et al.* (1996) for isolating diffuse emission from HII region emission. This technique compensates for the varying brightness of the DIG layer with radius in the galaxy and galaxy inclination (the reason a simple isophotal cut at a given surface brightness fails). The method involves subtracting smoothed version of the image from the original to remove the diffuse component, then making a mask on the resulting image which removes pixels greater than a certain value and replaces them with zero. The mask is applied to the original image to remove HII regions emission. The technique was tested by applying it to the M31 images of Walterbos & Braun (1992, 1994). We chose a scale of 900 pc for the median box used to smooth the image, and a cut level of 50 pc cm^{-6} to make the mask, because these parameters resulted in diffuse fractions similar to those that were found by manually cataloging and removing the HII regions by hand in M31. Note that the cut level of 50 pc cm^{-6} in the image after subtracting the smoothed version does not correspond to the same level in the original image.

We applied this technique to the galaxies in our sample. The measured diffuse fractions are given in table 3. Our $\text{H}\alpha$ flux NGC 4631 is low compared to Rand *et al.* (1992), so to test the effects of a possible calibration error we multiplied the image by 1.3 and recalculated the diffuse fraction using the same method, which gave 37–41%, very similar to the original value. The diffuse fractions for NGC 3003, NGC 4244, NGC 4631, and UGC 9242 all fall within the 30 to 50% range found for face-on galaxies (Hoopes *et al.* 1996; Greenawalt *et al.* 1998). NGC 891, however, shows a much higher fraction, 83–86%. The diffuse fraction for NGC 891 was measured on the 0.9 meter image. Applying the technique to the lower resolution Schmidt image gives a fraction of 90%. The difference between the fractions measured on the Schmidt and 0.9 meter images of NGC 891 is most likely due to unresolved HII regions in the lower resolution Schmidt image being counted as DIG.

Comparison of the diffuse fractions found in edge-on galaxies to those found in face-on systems is not straightforward. Since the HII region layer is confined to the midplane where the dust density is the highest, one might expect to measure a higher diffuse fraction in edge-on galaxies, as the HII regions would be affected more by the dust disk than they would in face-on galaxies. The DIG extends well out of the dust disk, especially in NGC 891, so much of it is less obscured. This may explain the high ratio in NGC 891. As the only Sb galaxy in our sample, it may have a higher metal content than the later type spirals, and the higher abundance of dust may obscure more of the disk HII region emission. A comparison of the $\text{H}\alpha$ surface brightness with the FIR surface brightness supports the

idea that NGC 891 contains more dust than the other galaxies in our sample. The FIR luminosity is an upper limit to the star formation rate, as an unknown fraction arises from dust heated by older stars. The $H\alpha$ luminosity gives a lower limit to the star formation rate, since it is affected by extinction. Table 3 shows that the $L_{H\alpha}/L_{FIR}$ ratio for NGC 891 is low relative to the other galaxies in the sample, implying higher extinction. Interestingly, NGC 4244 has a high value for this ratio, implying that it may be dust poor.

5. Line Ratios in NGC 4631

Figure 12 shows a subsection of the $H\alpha$ image of NGC 4631 and the $[OIII]/H\alpha$ and $[SII]/H\alpha$ ratio images. The figure shows a portion of the disk east of the bulge of the galaxy. In the $[OIII]/H\alpha$ image the cores of HII regions show a high ratio, while the DIG shows a lower ratio. Not all HII regions have high $[OIII]/H\alpha$ ratios, however, and in those that do only the central core has an elevated ratio, except for one region described below. The $[SII]/H\alpha$ image shows the opposite trend, with the DIG showing a higher $[SII]/H\alpha$ ratio than HII regions.

Applying the mask made on the $H\alpha$ image of NGC 4631 to the $[OIII]$ and $[SII]$ images allows us to investigate the line strengths in the DIG and in HII regions. The continuum in the bulge did not subtract well from the $[OIII]$ image, so we omitted that region and determined the ratio in the disk east and west of the bulge. The global $[SII]/H\alpha$ and $[OIII]/H\alpha$ ratios are given in table 6. The $[SII]/(H\alpha + [NII])$ ratio is elevated in the DIG, while $[OIII]/(H\alpha + [NII])$ is lower. Note that the $H\alpha$ filter also contains a contribution from the nearby $[NII]$ lines, which must be taken into account when comparing with other measurements. In the disk $[NII]/H\alpha$ varies from 0.1 to 0.2 in HII regions, and 0.3 to 0.5 in the DIG (Golla, Dettmar, & Domgörgen 1996). Thus when comparing to measurements made without $[NII]$, the observed $[OIII]/H\alpha$ and $[SII]/H\alpha$ ratios for NGC 4631 could be 1.1 to 1.2 times higher in HII regions, and 1.3 to 1.5 times higher in the DIG. Another important point is that the images are not corrected for internal extinction. Greenawalt *et al.* (1997) found that the extinction in HII regions is higher than that in the DIG in M31. If this is also true in NGC 4631 then correcting for extinction would reduce the $[OIII]/H\alpha$ ratio in HII regions more than in the DIG. The large uncertainties at high z distance, due to low signal in the $[OIII]$ and $[SII]$ images, prevent us from investigating the behavior of the line ratios away from the plane.

There is an extended region on the SE side of the disk where the $[OIII]/H\alpha$ ratio reaches over 1.0 (near the bottom of the images in figure 12). This is comparable to the ratios seen in the cores of HII regions, but the high $[OIII]$ gas appears more extended than

other HII regions, and lies in a region where the $\text{H}\alpha$ emission is about 180 pc cm^{-6} . By contrast, the cores of HII regions which show high [OIII] have emission measures of about 1500 pc cm^{-6} . This is the same location in the galaxy where Rand & van der Hulst (1993) found a large HI supershell. The shell has been modeled as a collision of a high velocity cloud with the disk of NGC 4631 (Rand & Stone 1996). The region of high [OIII] emission is about 650 pc in diameter, but borders on a large HII region which also shows high [OIII]/ $\text{H}\alpha$, so the true extent is difficult to measure. The ratios in a 370 pc wide vertical slice through the region are shown in figure 13. The location of this slice is marked in figure 12. The [SII]/ $\text{H}\alpha$ ratio in this region is about 0.2, close to the value in HII regions. The gas here may be shock ionized, which can produce a high [OIII]/ $\text{H}\alpha$ ratio (Shull & McKee 1979; Dopita & Sutherland 1995). Shock-ionized gas can also have low [SII]/ $\text{H}\alpha$ if the density is high enough to collisionally de-excite S^+ (Dopita & Sutherland (1995)). This region was not included in the determination of the global [OIII]/ $\text{H}\alpha$ and [SII]/ $\text{H}\alpha$ ratios.

6. Limits on Emission from the Outer Disk

One of the goals of this project was to detect or set limits on $\text{H}\alpha$ emission from the outer disk. These observations were driven by the recent discovery of sharp edges to the HI disks in nearby galaxies such as NGC 3198 (van Gorkom 1991). A possible explanation for these edges is that the outer Hydrogen is ionized, making it undetectable to 21 cm observations, as suggested by Silk & Sunyaev (1976). There are no ionizing stars at these large radii, and since the HI typically extends several kpc past the optical or $\text{H}\alpha$ disk any ionizing radiation from within the galaxy would surely be absorbed by the intervening HI. Therefore the ionizing source must be extragalactic, and is thought to be the metagalactic ionizing radiation field produced by quasars and AGN.

This idea has been modeled (Maloney 1993; Corbelli & Salpeter 1993; Dove & Shull 1994) and the observed cutoff can be reproduced. A crucial test, however, is to directly detect the ionized outer disk. The models indicate that the emission would be extremely faint, as low 0.05 pc cm^{-6} , but possibly as high as 0.2 pc cm^{-6} , depending on the gas density, clumpiness, and the strength of the ionizing radiation field. This is fainter than imaging studies have reached in the past. Ionized gas was detected in the outer disk of NGC 253 (Bland-Hawthorn *et al.* 1997) at a level of 0.23 pc cm^{-6} , using very sensitive Fabry-Perot observations. The emission would imply a metagalactic radiation field stronger than the current upper limit of $8 \times 10^{-23} \text{ ergs cm}^{-2} \text{ s}^{-1} \text{ Hz}^{-1} \text{ sr}^{-1}$ (Vogel *et al.* 1995), and the authors argue that the gas is photoionized by disk OB stars which can see the warped outer disk.

With extreme care in flatfielding, it may be possible to detect this level of emission through deep narrow-band imaging. Recently Donahue *et al.* (1995) detected a very faint halo around NGC 4631. The surface brightness of this halo is as high as 0.69 pc cm^{-6} , much brighter than that expected from the metagalactic radiation field, so the emission is most likely a result of the star formation activity in the galaxy or related to the gravitational interaction with its neighbors. We used similar imaging techniques in order to optimize the detection of faint emission. Our target galaxies (NGC 3003 and UGC 9242) were chosen to be at high galactic latitude so that they were not affected by many bright foreground stars or emission from the Reynolds layer. The sensitivity of the NGC 3003 image is about 2.0 pc cm^{-6} per square arcsecond, and about 2.7 pc cm^{-6} per square arcsecond for UGC 9242, much brighter than the strongest expected emission of 0.25 pc cm^{-6} found by Maloney (1993). In order to reach fainter levels, we spatially averaged over an ever increasing area to lower the noise until the limit of the flatfielding accuracy was reached and no further increase in S/N with smoothing was apparent. The NGC 3003 image was binned into 25×25 pixel ($17.3'' \times 17.3''$) boxes, which increased the sensitivity by a factor of 17.3 to 0.13 pc cm^{-6} . The UGC 9242 could be averaged over 30×30 pixel ($20.7'' \times 20.7''$) regions, increasing the sensitivity to 0.13 pc cm^{-6} . The rms intensity deviation between the background levels in boxes in flat regions of the image was equal to or less than this limit, even for boxes separated by large distances. The spatial scale for these limits are 2 kpc for NGC 3003 and 2.6 kpc for UGC 9242.

The binned images show no obvious outer disk emission. In figure 14 we show the major axis profiles of the two galaxies from the binned images. UGC 9242 has a distinct hole on the west side (positive major axis distance in figure 14). This appears to be a flatfielding error at the edge of one of the images which went into the final mosaic. Aside from this, any outer disk emission is below the limits of our flatfielding accuracy. We also smoothed using a median filter, using the same size median box as the average box used above. The NGC 3003 image shows no evidence for outer disk emission, but the UGC 9242 image has some interesting features (see figure 15). Faint extraplanar emission is visible on both sides of the disk. On the east side of the disk there is a bright star, which may account for the emission in this region. On the west side, however, the stars are fainter and less likely to contribute much scattered light. On this side the emission ranges from about 2 pc cm^{-6} at 2 kpc above the midplane to our limit of 0.13 pc cm^{-6} at 8.5 pc above the midplane. It appears that the emission is centered towards the nucleus, which may imply a connection to the central starburst, but might also just reflect the distribution of halo gas.

The H α disk also appears more extended in the median smoothed image. The H α emission extends about 8 kpc past the southern edge of the optical disk (the left side of figure 15). The optical edge is at about -21 Mpc in figure 14. Several factors lead us

to question the validity of this feature. The emission ranges in brightness from 0.16 to 0.20 pc cm^{-6} , just barely above our detection limit, making this a $1-2\sigma$ detection at best, and is not confirmed in the binned image. There is a background galaxy and some faint foreground stars which may affect the flatfielding in this region. There are other variations of similar magnitude near stars in the image. An example of this can be seen just below the extended disk in figure 15, where scattered light from a background galaxy and a group of several small stars created a spot in the smoothed image. Although stars are removed more cleanly during continuum subtraction in the deconvolved images than in the original images, there are still residuals due to effects such as a changing PSF across the field, leading to this further source of uncertainty for faint emission. If this emission were real, it would contradict the limits set by the NGC 3003 image, as well as other established upper limits on the metagalactic ionizing flux (see section 7.2).

7. Discussion

7.1. Halo Emission

We have detected the DIG layer in NGC 891 out to at least 5 kpc from the plane, and possibly as far as 7 kpc. NGC 891 has the brightest and largest DIG layer known, and it is not surprising to detect emission so far from the plane in a deep image. What is surprising is that UGC 9242, which shows much less extraplanar emission, still has a halo extending as far as 3 to 4 kpc, though significantly fainter than the NGC 891 halo. The image of UGC 9242 is of very high sensitivity, so it is possible that similar faint halos might be seen around other edge-ons even if they do not possess a bright DIG layer. We also confirm the existence of extraplanar emission in NGC 4631, although we could not have verified the halo claimed for NGC 4631 by Donahue *et al.* (1995). For the other galaxies in our sample, even in our very sensitive images of NGC 3003 and UGC 9242, we do not detect such a halo.

Excluding NGC 3003, which has too low an inclination to properly study the extraplanar emission, NGC 4631 and NGC 891 are the brightest in $\text{H}\alpha$, and they also show the most extraplanar emission of the sample. Although directly inferred star formation rates from the $\text{H}\alpha$ luminosity can be very unreliable for edge-on galaxies due to extinction, in a relative sense NGC 891 and NGC 4631 would appear to be the most actively star forming galaxies of the sample (again excluding NGC 3003). The extreme difference between these galaxies and NGC 4244, with its low $\text{H}\alpha$ luminosity and weak DIG layer, point to a link between active star formation and extraplanar emission, as discussed previously by Rand (1996). This conclusion is supported by the FIR luminosity (Rand 1996), which traces star formation more accurately than $\text{H}\alpha$ in edge-on galaxies, although some fraction of the FIR

emission may stem from dust heated by general starlight, not OB stars. In table 3 we list the FIR luminosity normalized by the square of the disk diameter (D_{25}), following Rand (1996). The galaxies with the highest current star formation have the most prominent extraplanar emission. This does not carry over to the diffuse fractions, however. In fact the diffuse fractions seem relatively constant with the exception of NGC 891, and this may be due to higher extinction in that galaxy. NGC 891 is the only Sb in the sample and may have a higher dust content than the rest of the sample (all Sc galaxies). The constancy of the diffuse fraction further reinforces the connection with star formation, since it essentially means that the DIG luminosity scales with the HII region luminosity. It is also interesting that there is not a more pronounced difference between face-on and edge-on diffuse fractions. This might imply that we are seeing most of the disk H α emission even in edge-on galaxies, with the exception of NGC 891. Diffuse fractions for more edge-on spirals are necessary to test this idea further.

The vertical profiles of NGC 891, UGC 9242, and possibly NGC 4244 are best described by two distinct exponential components, raising the possibility that more than one mechanism is responsible for creating H α halos. NGC 891 possesses a thick stellar disk, while NGC 4244 does not, which may suggest a connection between the mechanism which creates a thick disk and that which is responsible for the H α halo. However, a counter-example can be found in NGC 4565, which does possess a thick stellar disk (Morrison 1999), but has little extraplanar H α emission (Rand *et al.* 1992). An x-ray observation of NGC 891 (Bregman & Pildis 1994; Bregman & Houck 1997) revealed a halo of 10^6 K gas, with a distribution similar to the H α emission. The idea that hot supernovae-heated gas vented into the halo through chimneys is responsible for this emission led the authors to calculate whether the cooling of this hot gas could be the source of the H α emission. They found that the cooled gas mass was an order of magnitude too low to account for the mass of H α emitting gas. Rand (1997b) suggested that cooling gas may explain the more-extended halo component of the H α emission, while gas ionized by photons from OB stars leaking out of the disk is responsible for the brighter, less-extended component. The H α image of the DIG in UGC 9242 revealed a very extended halo component, but the scale height of the disk component is much lower than that of the similar component in NGC 891. Perhaps cooling gas could be responsible for a faint halo such as in UGC 9242, but some mechanism prevents the gas which makes up the disk component from reaching as high as in NGC 891. There is indication of an outflow into the halo from the nuclear filaments on both sides of the disk, which might provide a source of hot halo gas. Table 6 shows that the halo components in both UGC 9242 and NGC 4244 are much less prominent relative to the disk components than is true for NGC 891, where the two components are nearly equal. If cooling gas is responsible for the halo component,

NGC 891 must have a much more active chimney mode than UGC 9242 and NGC 4244.

Recently several galaxies have been observed to have high [OIII]/H α ratios in the DIG, including NGC 891 (Rand 1998). The implication is that a single ionization source cannot be responsible for both the low [OIII] and high [OIII] emitting gas, so another source of ionization is necessary. As Rand (1998) and Wang & Heckman (1997) point out, shock ionized gas can have high [OIII]/H α , so shocks may be an important mechanism for ionizing this component of the DIG. In NGC 891 the high [OIII] values are measured in the very high- z gas, suggesting that shock ionization or some other mechanism is important in the upper halo. In NGC 4631 we measure [OIII]/H α + [NII] ratios consistent with the DIG in several external galaxies (Greenawalt *et al.* 1997; Wang, Heckman, & Lehnert 1997), but higher than the Milky Way ratios. Photoionization models (*i.e.* Domgörgen & Mathis 1994) have been constructed which reproduce the Galactic values, so they underpredict the [OIII] in NGC 4631. The [OIII]/H α ratio seen in the DIG of M31 (Greenawalt *et al.* 1997) is similar to those we find for NGC 4631. Those authors found that a model adjusted so that the ionizing radiation is less diluted on average could reproduce the observed ratios. A similar situation may exist in NGC 4631, where the overall star formation is enhanced in the disk. It then appears that photoionization is the only ionization mechanism necessary for NGC 4631, in the disk at least. The sensitivity at high z in the [OIII] and [SII] images is not good enough to determine the ratio, so a trend such as that in NGC 891 may well exist.

7.2. Outer Disk Emission

Our efforts to detect the outer disk H α emission allow us to set an upper limit on the metagalactic ionizing radiation field. Maloney (1993) constructed a model of the ionization of the outer disk of NGC 3198 by the metagalactic radiation field. The model predicts a range of expected H α surface brightness for different values of the ionizing flux. An important result from the model was that the predictions are insensitive to galaxy parameters, so we can apply the results for NGC 3198 to the galaxies in our sample. The models assume that the gas is smoothly distributed; if the gas is clumpy the emission will be brighter.

Comparison of our upper limit on the H α emission of 0.13 pc cm^{-6} for the outer disk of NGC 3003 with the predicted emission measure in Maloney (1993, see their figure 14) shows that the upper limit on the metagalactic ionizing flux J_ν is between 8 and $12 \times 10^{-23} \text{ ergs cm}^{-2} \text{ s}^{-1} \text{ Hz}^{-1} \text{ sr}^{-1}$. The calculations in Maloney (1993) are based on the observed sharp cutoff in the HI disk at large radii. The scenario is one in which the HI disk dips below a critical column density where it becomes optically thin to the metagalactic ionizing flux,

going from a mostly neutral disk to a mostly ionized disk. Vogel *et al.* (1995) set a limit on extragalactic H α emission using Fabry-Perot observations of an intergalactic Hydrogen cloud. They placed a 2σ limit on the metagalactic ionizing flux to 8×10^{-23} ergs cm $^{-2}$ s $^{-1}$ Hz $^{-1}$ sr $^{-1}$, in agreement with the result presented here. Donahue *et al.* (1995) found that $J_\nu < 3.3 \times 10^{-23}$ ergs cm $^{-2}$ s $^{-1}$ Hz $^{-1}$ sr $^{-1}$, by imaging intergalactic Hydrogen clouds in H α , more stringent than our limit.

A simple check of these numbers can be made by calculating the number of ionizing photons required to produce the observed H α emission. An emission measure of 0.13 pc cm $^{-6}$ requires 8×10^4 photons cm $^{-2}$ s $^{-1}$, assuming the HI is optically thick to ionizing photons and that 45% of ionizing photons result in H α photons (Case B). The current limit is 6×10^4 photons cm $^{-2}$ s $^{-1}$ for two-sided incident ionizing flux (Vogel *et al.* 1995). This would imply that our limit is a factor of 1.3 higher, so $J_\nu < 11 \times 10^{-23}$ ergs cm $^{-2}$ s $^{-1}$ Hz $^{-1}$ sr $^{-1}$. We have not quite reached the limits set by Fabry-Perot observations nor that set by H α imaging of Hydrogen clouds, so it is not surprising that we do not detect any outer disk emission from NGC 3003. It is important to remember that the conversion from H α emission measure to metagalactic ionizing flux assumes that no [NII] is present. The filter used here may transmit [NII] at the 10–20% level. This is normally a small percentage of H α , but it could be significant if the [NII]/H α ratio is very high in the outer disk, as was found by Bland-Hawthorn *et al.* (1997) for NGC 253.

In UGC 9242 there is an indication of outer disk H α emission at the 0.16 pc cm $^{-6}$ level. If this emission were a result of the metagalactic ionizing radiation field, it would require that $J_\nu = 17.0 \times 10^{-23}$ ergs cm $^{-2}$ s $^{-1}$ Hz $^{-1}$ sr $^{-1}$, higher than the Vogel *et al.* (1995) upper limits, and higher than the limit set by NGC 3003. The presence of several foreground stars and a background galaxy at this location in the image lead us to question whether this feature is real. It could be either the result of flatfielding errors, or it could be real emission but powered by some source other than the metagalactic ionizing radiation field.

We thank the KPNO staff for their help during these observing runs. We also thank B. Greenawalt for observing NGC 891, and M. F. Steakley for reducing the NGC 4244 and NGC 4631 images. We thank the referee, James Schombert, for useful comments which improved the presentation of the results. This research was supported by the NSF through grant AST-9617014, and by a Cottrell Scholar Award from Research Corporation. C.G.H. was supported by a grant from the New Mexico Space Grant Consortium.

REFERENCES

Bland-Hawthorn, J., Freeman, K. C., & Quinn, P. J. 1997, *ApJ*, 490, 143

Bregman, J. N. & Houck, J. C. 1997, *ApJ*, 485, 159

Bregman, J. N. & Pildis, R. A. 1994, *ApJ*, 420, 570

Burstein, D. & Heiles, C 1994, *ApJS*, 54, 33

Corbelli, E. & Salpeter, E. E. 1993, *ApJ*, 419, 104

Corbelli, E., Schneider, S. E., & Salpeter, E. E. 1989, *AJ*, 97, 390

Dettmar, R.-J. 1990. *A&A*, 232, L15

Domgörgen, H., & Mathis, J. S. 1994, *ApJ*, 428, 647

Donahue, M., Aldering, G., & Stocke, J. T. 1995 *ApJ*, 450, L45

Dopita, M. A., & Sutherland, R. S. 1995, *ApJ*, 455, 468

Dove, J. B., & Shull, J. M. 1994, *ApJ*, 423, 196

Ferrara, A., Bianchi, S., Dettmat, R.-J., & Giovanardi, C. 1996, *ApJ*, 467, L69

Ferguson, A. M. N., Wyse, R. F. G., Gallagher, J. S., Hunter, D. A. 1996, *AJ*, 111, 2265

Golla, G., Dettmar, R.-J., & Domgörgen, H. 1996, *A&A*, 313, 439

Greenawalt, B., Walterbos, R. A. M., & Braun, R. 1997, *ApJ*, 483, 666

Greenawalt, B., Walterbos, R. A. M., Thilker, D. & Hoopes, C. G. 1998, *ApJ*, 506, 135

Hester, J. J., Kulkarni, S. R., Rand, R. J., & Deich, W. T. 1990, in *The Interstellar Disk-Halo Connection in Galaxies*, IAU Symposium No. 144, edited by H. Bloemen (Dordrecht:Kluwer), 51

Heckman, T. M., Armus, L., & Miley, G. K. 1990, *ApJS*, 74, 833

Hoopes, C. G., Walterbos, R. A. M., & Greenawalt, B. E. 1996, *AJ*, 112, 1429

Kennicutt, R. C. 1988, *ApJ*, 334, 144

Kennicutt, R. C. 1992, *ApJ*, 388, 310

Kulkarni, S. R., & Heiles, C. 1988, in *Galactic and Extragalactic Radio Astronomy*, ed. G. L. Versuur & K. I. Kellerman (New York:Springer-Verlag), 95

Maloney, P. 1993, *ApJ*, 414, 41

Mathis, J. S. 1986, *ApJ*, 301, 423

Martin, C. L. 1997, *ApJ*, 491, 561

Morrison, H. L., Miller, E. D., Harding, P., Stinebring, D. R., & Boroson, T. A. 1997, AJ, 113, 2061

Morrison, H. L. 1999, in The Third Stromlo Symposium: The Galactic Halo, ed B. K. Gibson, T. S. Axelrod, & M. E. Putman (San Francisco:ASP), preprint

Olling, R. P. 1996, AJ, 112, 457

Pildis, R. A., Bregman, J. N., & Schombert, J. M. 1994, ApJ, 423, 190

Rand, R. J. 1996, ApJ 462, 712

Rand, R. J. 1997a, in The Interstellar Medium in Galaxies, ed. J. M. van der Hulst (Dordrecht:Kluwer), 105

Rand, R. J. 1997b, ApJ 474, 129

Rand, R. J. 1998, ApJ, 501, 137

Rand, R. J., Kulkarni, S. R., & Hester, J. J. 1990, ApJ, 352, L1 (RKH)

Rand, R. J., Kulkarni, S. R., & Hester, J. J. 1992, ApJ, 396, 97

Rand, R. J., & Stone, J. M. 1996, AJ, 111, 190

Reynolds, R. J. 1985, ApJ, 298, L27

Reynolds, R. J. 1989, in The Galactic and Extragalactic Background Radiation, IAU Symposium No. 139, ed. S. Bowyer and C. Leinert,(Dordrecht:Kluwer), 157

Reynolds, R. J. 1990, in The Interstellar Disk-Halo Connection in Galaxies, IAU Symposium No. 144, edited by H. Bloemen (Dordrecht:Kluwer), 67

Reynolds, R. J., & Tufte, S. L. 1995, ApJ, 439, L17

Rice, W., Lonsdale, C. J., Soifer, B. T., Neugebauer, G., Kopan, E. L., Lloyd, L. A., De Jong, T., & Habing, H. J. 1988, ApJS, 68, 91

Rupen, M. P. 1991, AJ, 102, 48

Silk, J. & Sunyaev, R. A. 1976, Nature, 260, 508

Shull, J. M., & McKee, C. F. 1979, ApJ, 227, 131

Tully, R. B. 1988, *Nearby Galaxies Catalog* (Cambridge: Cambridge University Press)

van Gorkom, J. H. 1991 in Atoms, Ions and Molecules: New Results in Spectral Line Astrophysics, ed. A. D. Haschick & P. T. P. Ho (San Francisco:ASP), p1

Veilleux, S., Cecil, G., & Bland-Hawthorn, J. 1995, ApJ 445, 152

Vogel, S. N., Weymann, R., Rauch, M., & Hamilton, T. 1995, ApJ, 441, 162

Walterbos, R. A. M. 1991, in The Interstellar Disk-Halo Connection in Galaxies, IAU Symposium No. 144, edited by H. Bloemen (Dordrecht:Kluwer), p223

Walterbos, R. A. M., & Braun, R. 1992, A&AS, 92, 625

Walterbos, R. A. M., & Braun, R. 1994, ApJ, 431, 156

Walterbos, R. A. M., & Braun, R. 1996, in ASP Conf. Proc. 106, The Minnesota Lectures on Extragalactic Neutral Hydrogen, ed. E. D. Skillman (San Francisco:ASP), 1

Wang, Q. D., Walterbos, R. A. M., Steakley, M. F., Norman, C. A., & Braun, Robert 1995, ApJ, 439, 176

Wang, J., Heckman, T. M., & Lehnert, M. D. 1997, ApJ, 491, 114

Young, J. S., Allen, L., Kenney, J. D. P., Lesser, A., & Rownd, B. 1996, AJ, 112, 1903

Table 1. Galaxy Parameters^a

Galaxy	Type	RA (2000)	dec (2000)	Distance (Mpc)	inclination (°)	D ₂₅ (arcmin)
NGC 891	Sb	2h19.3m	42°.07	9.5	89 ^b	12.2
NGC 3003	SBbc	9h45.6m	2°.51	24.4	90 ^c	6.0
NGC 4244	Scd	12h15.0m	38°.05	3.1	90	15.8
NGC 4631	Scd	12h39.8m	32°.49	6.9	85	14.7
UGC 9242	Scd	14h23.3m	39°.45	26.3	90	5.0

^aFrom Tully 1988, except where otherwise noted.

^bFrom Rupen 1991.

^cThe inclination of NGC 3003 appears to be less than that listed in Tully 1988.

Table 2. Observations

Galaxy	Filter ^a	Telescope	Date	Integration Time (Hours)	RMS Noise ^b (EM arcsec ⁻²)	PSF Radius ^c (arcsec)
NGC 891	H α 6580/28	Schmidt	1995 Nov	3.3	2.3	8.1
	H α 6580/28	0.9m	1996 Jan	1.3	5	4.8
NGC 3003	H α 6590/28	0.9m	1997 Mar	10.8	1.6	4.1
NGC 4244	H α 6569/29	0.9m	1992 Mar	1.5	4.5	3.7
NGC 4631	H α 6568/74	0.9m	1991 Feb	2.8	4	3.9
	[SII] 6744/84	0.9m	1991 Feb	1.7	6	3.9
UGC 9242	[OIII] 5024/55	0.9m	1991 Feb	1.8	11	4.7
	H α 6590/28	0.9m	1997 Mar	10.2	2.0	4.1

^aThe name of the line is given, as well as the central wavelength and FWHM in Å.

^bRefers to the continuum subtracted image.

^cThe radius which encircles 95% of the energy from a point source (foreground star).

Table 3. H α Properties

Galaxy	$L_{H\alpha}^a$ (10^{40} erg s $^{-1}$)	Diffuse Fraction ^b	$L_{H\alpha}/D_{25}^2$ (10^{37} ergs s $^{-1}$ kpc $^{-2}$)	L_{FIR}/D_{25}^2 ^c (10^{40} ergs s $^{-1}$ kpc $^{-2}$)
NGC 891	3.3 ± 0.3	83-86%	2.9	4.3
NGC 3003	11.8 ± 0.6	49-51%	6.1	8.0
NGC 4244	0.42 ± 0.02	44-49%	2.1	0.19
NGC 4631 ^d	14.3 ± 0.2	38-42%	16.4	3.5
UGC 9242 ^e	2.8 ± 0.2	46-50%	1.9	...

^aThe uncertainty is found by varying the continuum subtraction by $\pm 3\%$.

^bThe range is found by varying the continuum subtraction. The fractions are not corrected for internal extinction, which may account for the large fraction in NGC 891.

^cIRAS FIR fluxes are from Rice *et al.* 1988.

^dThe H α filter used for NGC 4631 also contains [NII].

^eUGC 9242 was not detected by IRAS.

Table 4. Exponential Model Fits to the Vertical EM Profiles^a

z direction	First Exponential		Second Exponential		Reduced χ^2
	EM _{midplane} ^b	Scale Height	EM _{midplane} ^b	Scale Height	
NGC 891, Central 10 kpc					
East	64	430	45	870	0.91
West	105	520	25	1350	0.93
East	87	710	1.02
West	94	850	1.59
NGC 4244, Central 10 kpc					
North	180	130	7	450	0.92
South	40	200	2	860	0.77
North	25	300	1.11
South	10	450	1.14
UGC 9242, Central 10 kpc					
North	230	180	10	1150	1.71
South	100	240	5	1700	1.20
North	87	380	5.50
South	44	500	5.08
UGC 9242, Central 20 kpc, excluding nucleus					
North	300	180	3	1900	1.01
South	130	270	4	2400	1.07
North	160	250	5.55
South	75	410	7.11

^aFor each galaxy, the first two rows give the results for the model using two exponential functions, and the third and fourth rows give the results for a single exponential function.

^bThis is the emission measure of the line of sight through the center of the disk (z=0), extrapolated from the vertical profile.

Table 5. Average DIG Parameters for Central 10 kpc

Galaxy	DIG Diameter (kpc)	Thick Disk EM _⊥ ^a (pc cm ⁻⁶)	Halo EM _⊥ ^a (pc cm ⁻⁶)	Total EM _⊥ ^a (pc cm ⁻⁶)	Surface Density (M _⊙ pc ⁻²)
NGC 891	15	5.5	4.9	10.4	$5.1(\phi/0.25)^{1/2}$
NGC 4244	11	2.9	0.5	3.4	$1.5(\phi/0.25)^{1/2}$
UGC 9242	20	3.3	1.0	4.3	$2.6(\phi/0.25)^{1/2}$
Galaxy ^b	4.5	2.6

^aEmission measure perpendicular to the disk, calculated by integrating the two-component exponential functions in table 4.

^bFrom Reynolds 1989.

Table 6. NGC 4631 Line Ratios in the Disk^a

Line	HII Regions	DIG
[SII]/(H $α$ +[NII])	0.26	0.41
[OIII]/(H $α$ +[NII])East	0.42	0.26
[OIII]/(H $α$ +[NII])West	0.53	0.14

^aNot corrected for extinction.

Fig. 1.— Left: The continuum-subtracted $\text{H}\alpha$ image of NGC 891, taken with the Burrell Schmidt. Right: A section of the KPNO 0.9 meter $\text{H}\alpha$ image of the same galaxy, showing the central 16 kpc of the galaxy. North is up and east is to the left in this and all other images, unless otherwise indicated. The bar in the lower left corner is 1 kpc at the distance of NGC 891.

Fig. 2.— Top: The red continuum image of NGC 3003. Bottom: The continuum subtracted $\text{H}\alpha$ image of the same galaxy. The bar in the lower left corner is 2 kpc at the distance of NGC 3003

Fig. 3.— The continuum subtracted $\text{H}\alpha$ image of NGC 4244. The bar in the lower left corner is 1 kpc at the distance of NGC 4244.

Fig. 4.— The continuum subtracted $\text{H}\alpha + [\text{NII}]$ image of NGC 4631. The bar in the lower left corner is 1 kpc at the distance of NGC 4631. The arrows indicate the large loop extending 3.5 kpc into the halo.

Fig. 5.— Top: The red continuum image of UGC 9242. Bottom: The continuum subtracted $\text{H}\alpha$ image of the same galaxy. The bar in the lower left corner is 2 kpc at the distance of UGC 9242.

Fig. 6.— A comparison of the DIG layers in the galaxies in our sample. The images have been rotated so the disk is horizontal; see figures 1–5 for the correct orientation. The images all have the same spatial scale, shown by the 1 kpc bar in the bottom panel. They are all displayed with the same logarithmic stretch, from -2 to 1000 pc cm^{-6} .

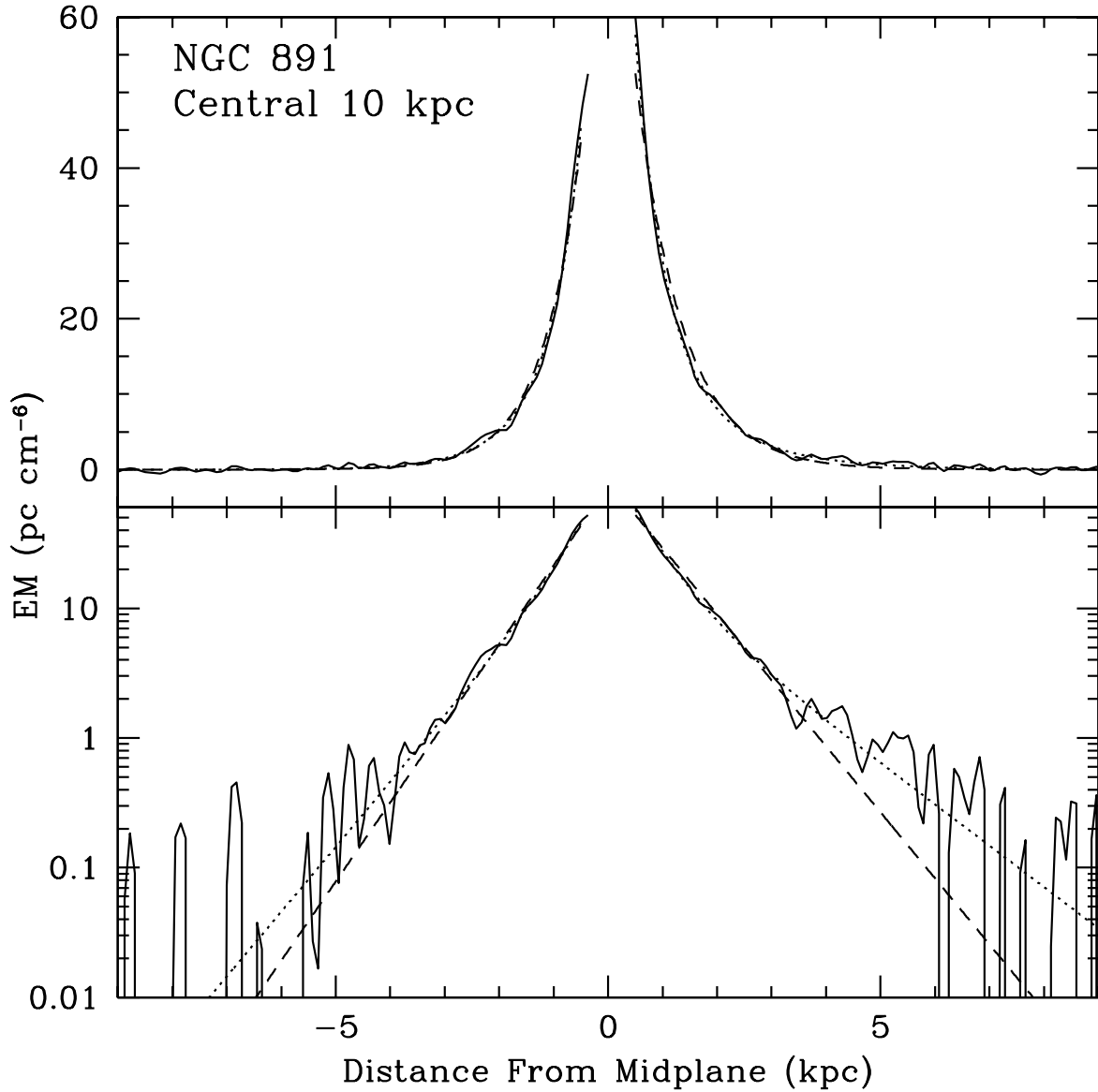


Fig. 7.— Vertical profile of the central 10 kpc of NGC 891. The top panel is linearly scaled, and the bottom panel is logarithmically scaled. Both the two-exponential fit (dotted line) and the single exponential fit (dashed line) from table 4 are shown.

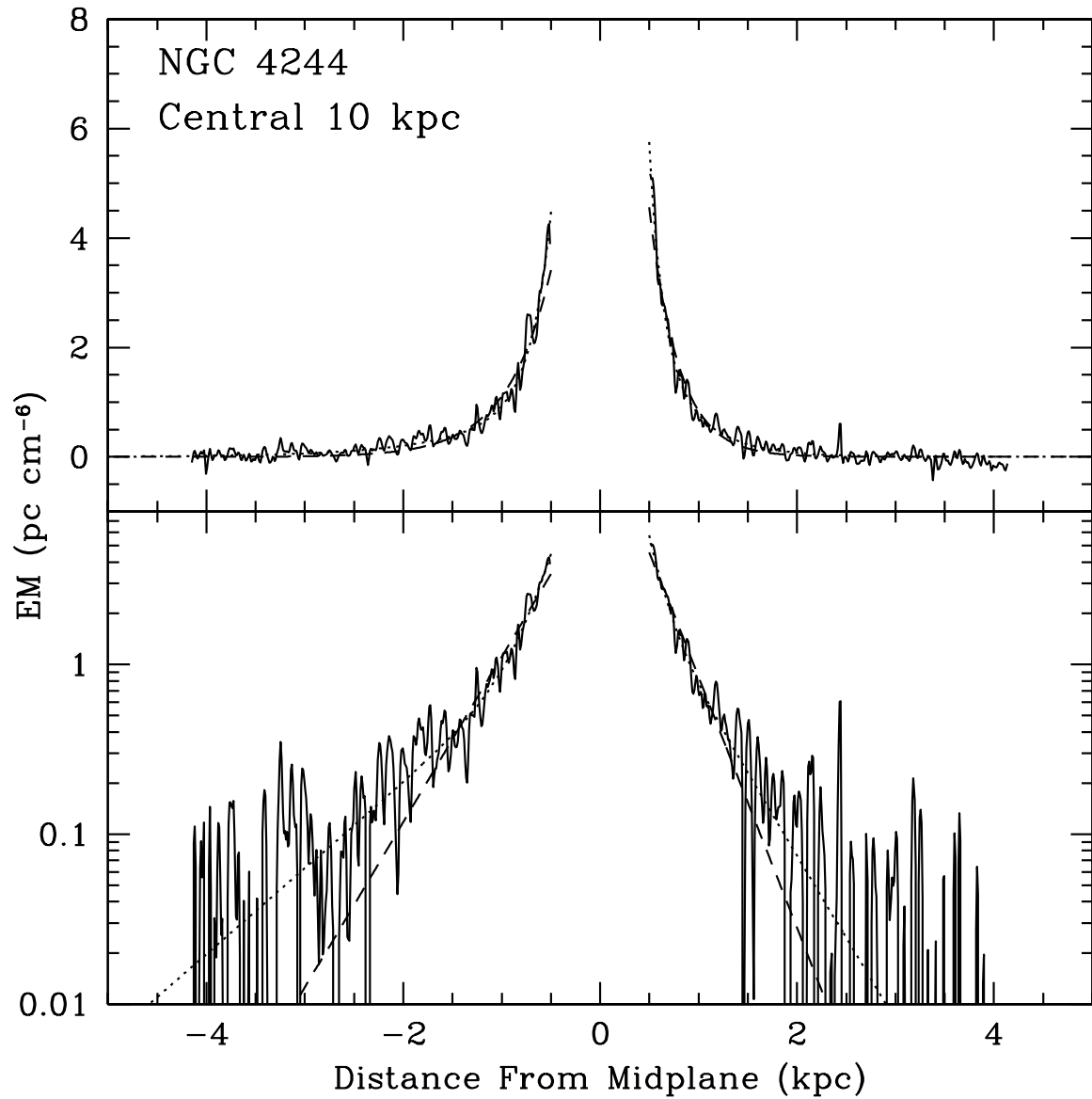


Fig. 8.— Vertical profile of the central 10 kpc of NGC 4244. Both the two-exponential fit (dotted line) and the single exponential fit (dashed line) from table 4 are shown.

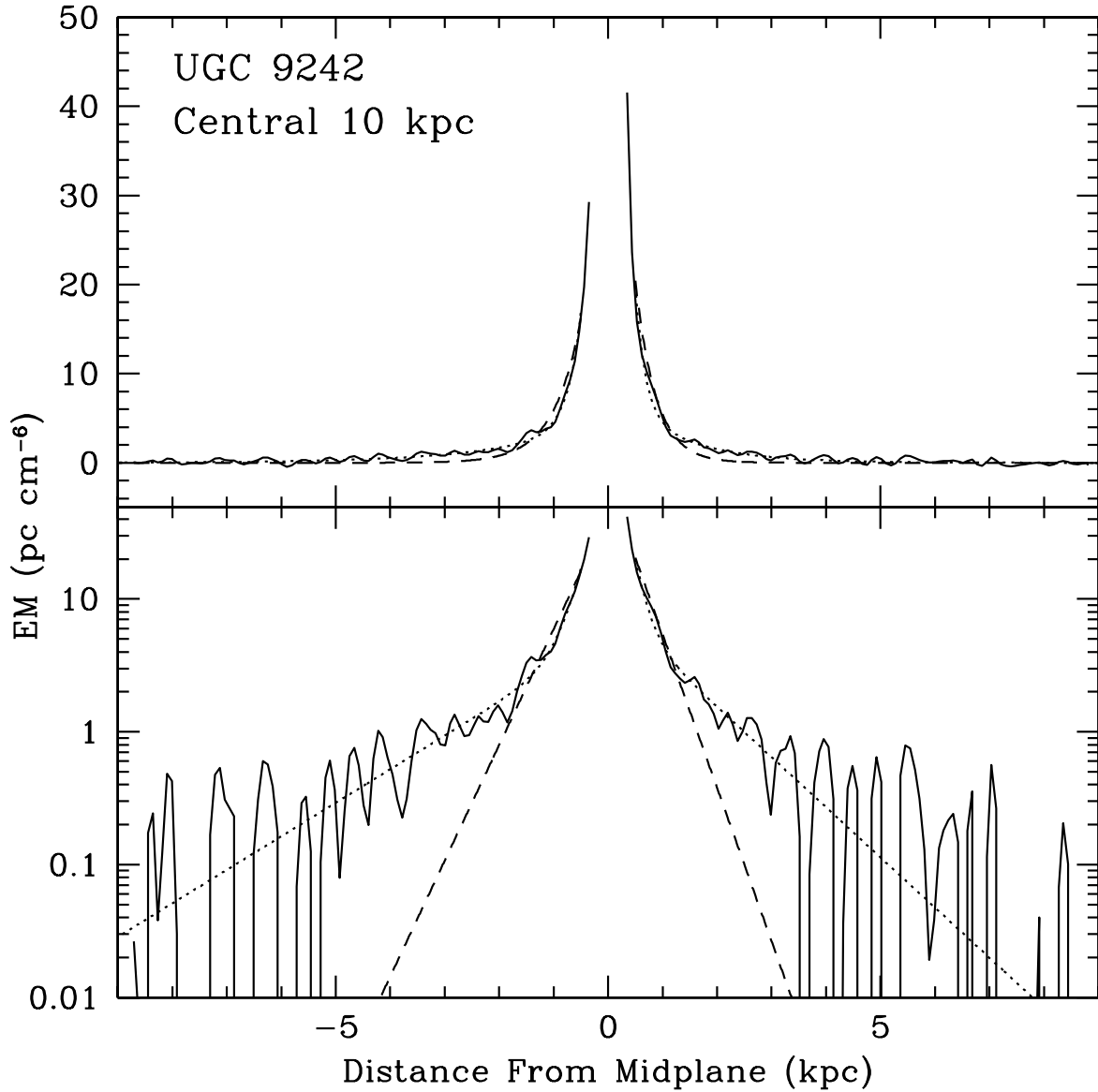


Fig. 9.— Vertical profile of the central 10 kpc of UGC 9242. Both the two-exponential fit (dotted line) and the single exponential fit (dashed line) from table 4 are shown.

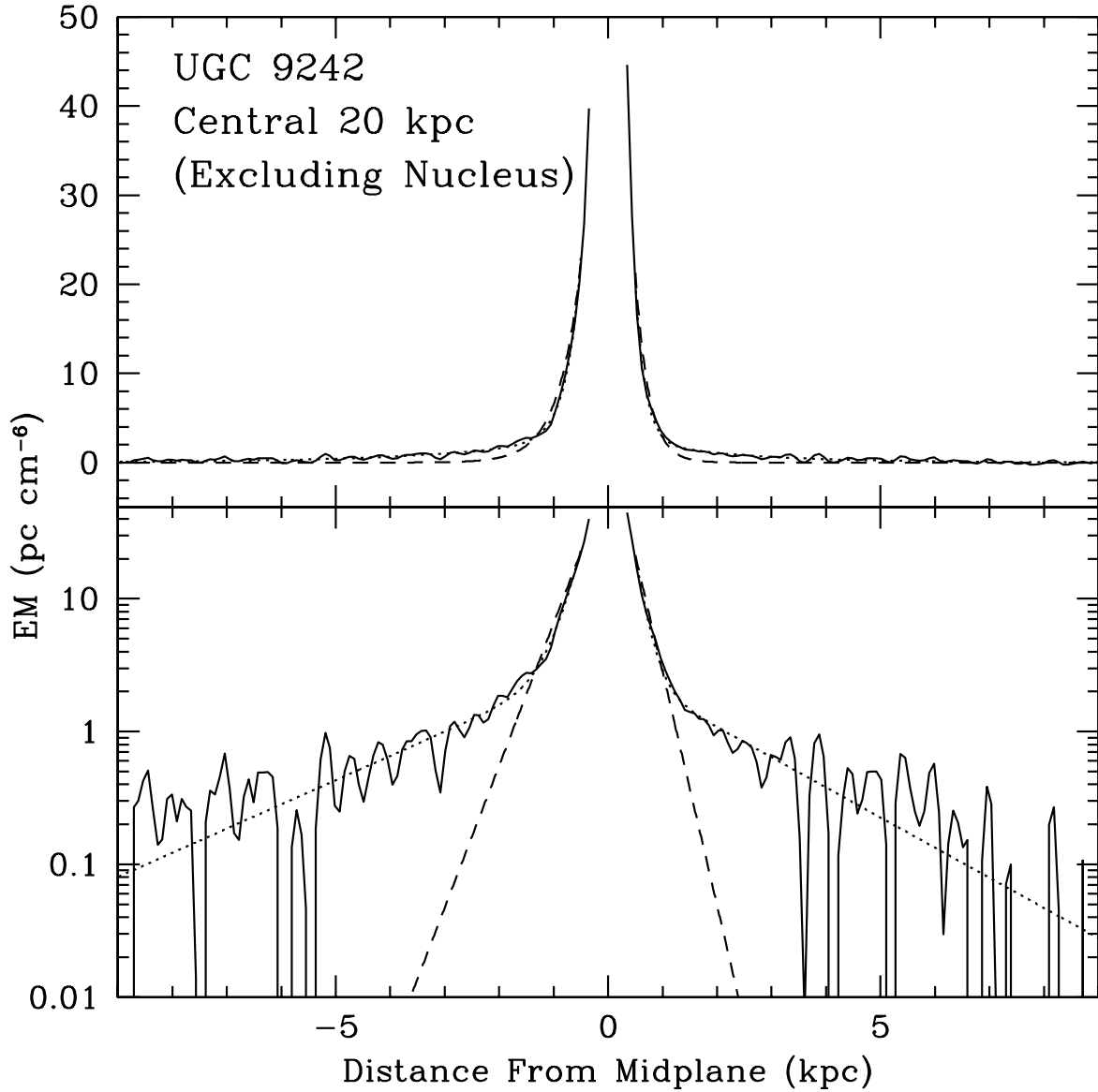


Fig. 10.— Vertical profile of the central 20 kpc of UGC 9242, with the central 3 kpc excluded. Both the two-exponential fit (dotted line) and the single exponential fit (dashed line) from table 5 are shown.

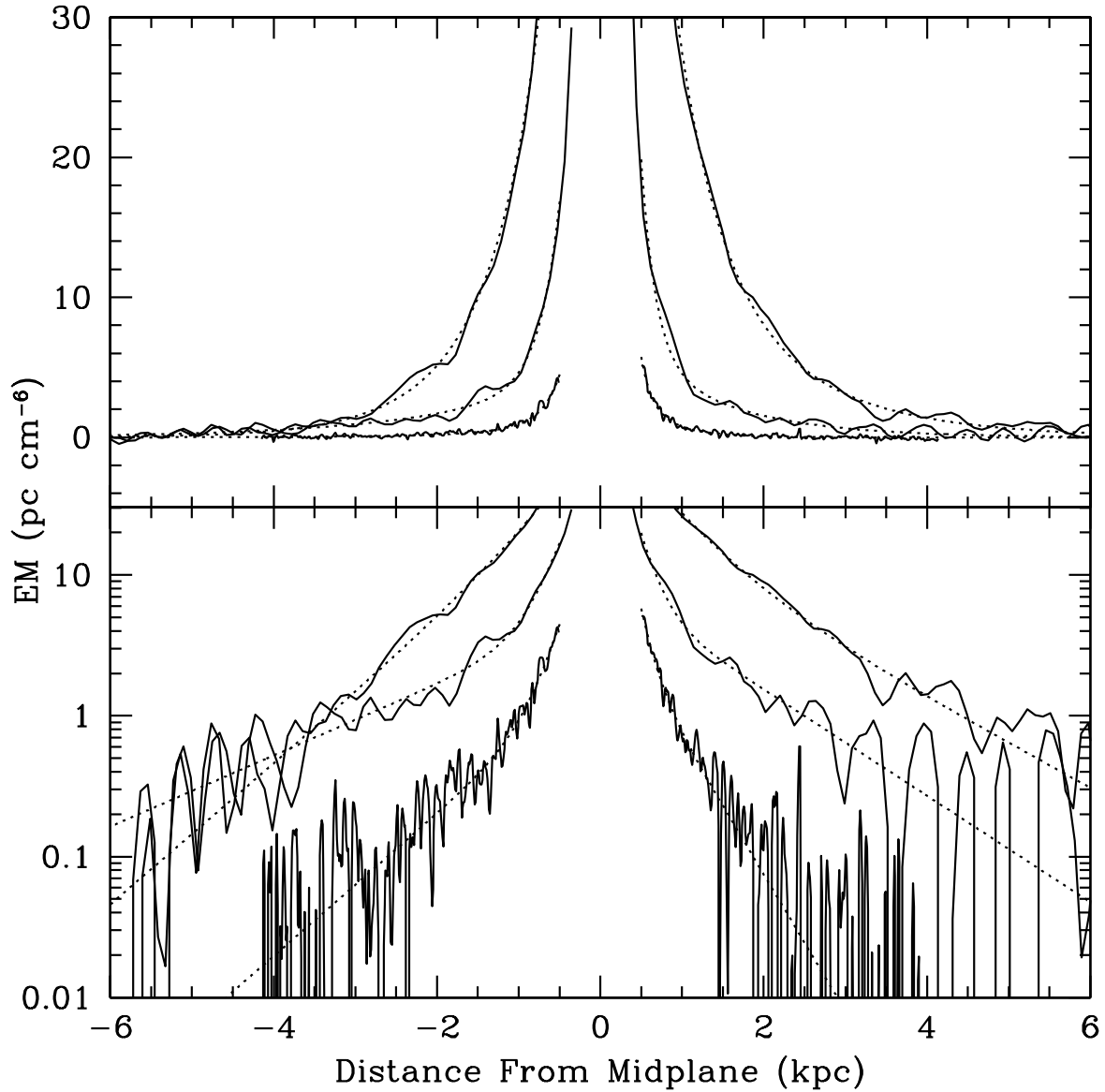


Fig. 11.— Vertical profile of the central 10 kpc of all three galaxies, shown in linear and logarithmic scale. The two-exponential fits from table 4 (dotted line) are shown.

Fig. 12.— A subsection of NGC 4631 showing the disk east of the bulge. The top panel is $\text{H}\alpha$, the middle is $[\text{OIII}]/\text{H}\alpha$, and the lower panel is $[\text{SII}]/\text{H}\alpha$. Note that the $\text{H}\alpha$ image also contains $[\text{NII}]$ emission. The $[\text{OIII}]/\text{H}\alpha$ image is scaled linearly from 0 to 1.2, and the $[\text{SII}]/\text{H}\alpha$ image is scaled linearly from 0 to 0.6. White represents high values in all three panels. The horizontal bar represents 1 kpc, and the vertical lines show the region of these images plotted in figure 13.

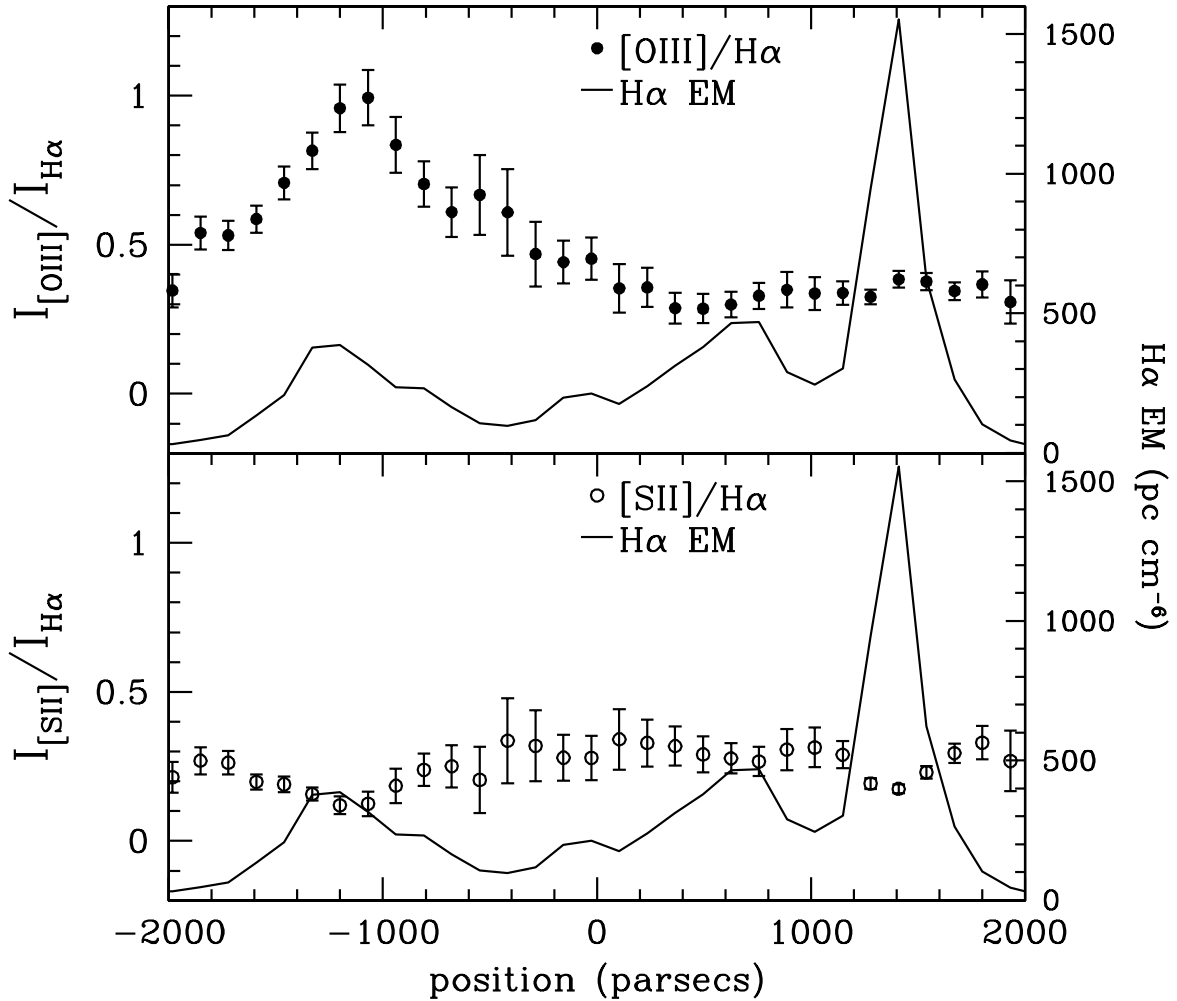


Fig. 13.— The H α surface brightness (solid line), [OIII]/H α ratios (filled circles in the top panel) and [SII]/H α ratio (open circles in the bottom panel) in a 370 pc wide vertical slice through NGC 4631 (see figure 12). The slice passes through the high [OIII] emitting gas which may be related to an HI supershell (see text). The region is at about -700 to -1500 parsecs in this plot. Note that the H α image contains [NII] emission.

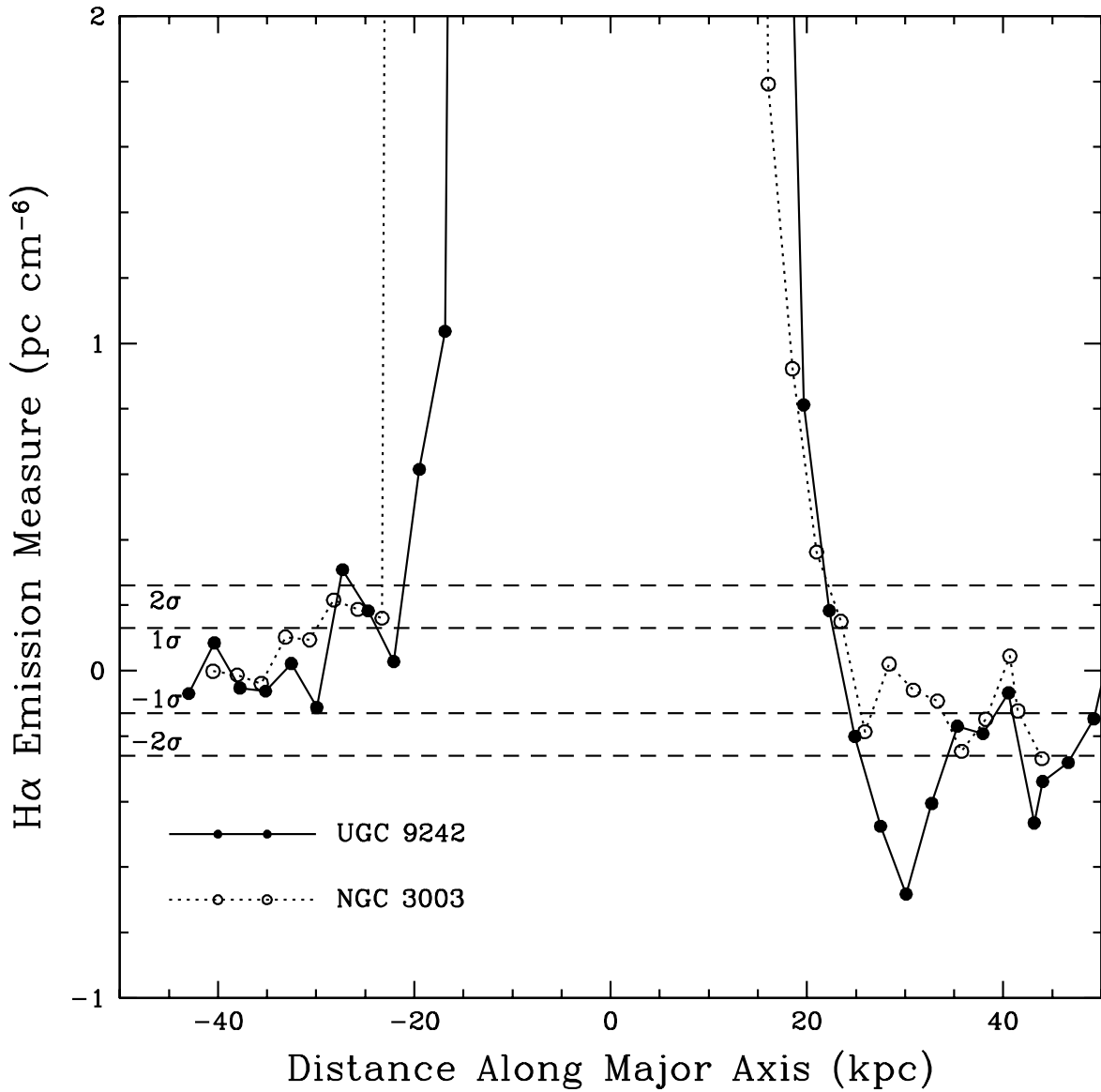


Fig. 14.— The major axis profiles of UGC 9242 (solid line) and NGC 3003 (dotted line). The images were binned in $2.6 \text{ kpc} \times 2.6 \text{ kpc}$ boxes for UGC 9242 and $2 \text{ kpc} \times 2 \text{ kpc}$ boxes for NGC 3003, in accordance with the limits on flatfielding accuracy found in section 6. The 1 and 2σ flatfielding accuracy levels are also shown.

Fig. 15.— A median filtered image of UGC 9242 (bottom panel) compared with the original H α +continuum image (top panel). The median box used was $20.7'' \times 20.7''$. Halo emission on both sides of the disk is apparent. Scattered light from a bright star below the disk may be a problem, but no such problem exists on the north side. The upper image shows the galaxy responsible for the dark smudge in the upper left corner of the image, as well as other galaxies and foreground stars that show up in the smoothed image. Features in this image are discussed in more detail in the text.

This figure "figure01.jpg" is available in "jpg" format from:

<http://arxiv.org/ps/astro-ph/9904154v1>

This figure "figure02.jpg" is available in "jpg" format from:

<http://arxiv.org/ps/astro-ph/9904154v1>

This figure "figure03.jpg" is available in "jpg" format from:

<http://arxiv.org/ps/astro-ph/9904154v1>

This figure "figure04.jpg" is available in "jpg" format from:

<http://arxiv.org/ps/astro-ph/9904154v1>

This figure "figure05.jpg" is available in "jpg" format from:

<http://arxiv.org/ps/astro-ph/9904154v1>

This figure "figure06.jpg" is available in "jpg" format from:

<http://arxiv.org/ps/astro-ph/9904154v1>

This figure "figure12.jpg" is available in "jpg" format from:

<http://arxiv.org/ps/astro-ph/9904154v1>

This figure "figure15.jpg" is available in "jpg" format from:

<http://arxiv.org/ps/astro-ph/9904154v1>